Review

Underwater Optical Communications: From Photodiodes to Single-Photon Detectors

Zbigniew Bielecki and Janusz Mikołajczyk *

Posted Date: 2 June 2026

doi: 10.20944/preprints202606.0076.v1

Keywords: optical wireless communication; underwater communications; photon counting

 doi:10.20944/preprints202606.0076.v1

Review

Underwater Optical Communications: From Photodiodes to Single-Photon Detectors

Zbigniew Bielecki and Janusz Mikołajczyk *

Institute of Optoelectronics, Military University of Technology, 00-908 Warsaw, Poland

* Correspondence: janusz.mikolajczyk@wat.edu.pl

Abstract

This paper reviews key hardware components of underwater wireless optical communications (UWOC) , with particular emphasis on photodetectors (PD). The growing demand for high-speed, low-latency underwater data links, driven by applications in autonomous underwater vehicle (AUV) networks, environmental monitoring, offshore exploration, and tactical surveillance, motivates a systematic comparison of available device technologies and their suitability across different deployment scenarios. The paper first outlines the fundamental constraints imposed by the aquatic optical channel, including wavelength-dependent absorption and scattering, turbulence-induced intensity fluctuations, and their combined impact on achievable link range and data rate. The spectral transmission window of water in the 450–550 nm range is identified as the primary wavelength constraint for selecting the light sources and photodetectors. It also includes a brief overview of radiation sources used in UWOC systems. The operating principles, modulation bandwidths, and beam characteristics of light-emitting diodes (LEDs) and laser diodes (LDs), have been compared. In the main part, the review focuses on analyzing the UWOC receiver's construction across five PD's technologies: photomultiplier tubes (PMTs), p-i-n photodiodes (PINs), avalanche photodiodes (APDs), single-photon avalanche diodes (SPADs), and silicon photomultipliers (SiPMs/MPPCs). For each technology, the operating principle, gain mechanism, and key parameters, including responsivity, noise-equivalent power, bandwidth, and bias requirements, are described and linked to reported experimental UWOC results. The analysis covers both analog and photon-counting reception modes, as well as advanced modulation and signal-processing techniques that extend link reach and throughput. The analysis of PD technologies for their suitability for underwater optical communication systems constitutes a unique data source for technologists and designers. It highlights experimental results from many researchers across various PD types and modulation formats. A fundamental trade-off between receiver sensitivity and data rate is observed, e.g., PINs achieve the highest data rates (up to ~25 Gbps over short distances) but have the lowest sensitivity, whereas single SPADs and PMTs offer the highest sensitivity (down to approximately −85 dBm) at the cost of reduced bandwidth. SiPM/MPPC arrays are identified as a promising intermediate technology, combining high single-photon sensitivity, spectrally efficient modulation formats, and low-bias-voltage operation. Emerging photodetector technologies, including perovskite-based photodetectors, SiC photoelectrochemical devices, and large-area scintillating-fiber receivers, are also reviewed as promising candidates for next-generation UWOC and Internet of Underwater Things deployments.

Keywords: optical wireless communication; underwater communications; photon counting

1. Introduction

Underwater wireless communication plays a crucial role in applications such as tactical surveillance, environmental monitoring, offshore exploration, and the operation of autonomous underwater vehicles (AUVs). The exploration and monitoring of marine environments require reliable data transmission capabilities; however, the underwater channel poses significant challenges

 doi:10.20944/preprints202606.0076.v1

for wireless communication because of strong attenuation, multipath propagation, and environmental variability [1,2]. Historically, underwater signaling relied primarily on acoustic methods, with early concepts dating back to Leonardo da Vinci in 1490. Despite their long-established use, modern underwater applications increasingly demand higher bandwidth, lower latency, and improved support for real-time data transfer, which has stimulated the development of radio frequency (RF) and UWOC systems. Traditionally, underwater communication has been dominated by acoustic and RF technologies, each characterized by specific physical limitations [3].

Acoustic systems can transmit over distances from several kilometers to several hundred kilometers under favorable conditions. For this reason, they remain indispensable for applications that require extended coverage. However, their practical usefulness is limited by low data rates, narrow bandwidth, high latency, and susceptibility to multipath fading and environmental interference [4].

RF communications represents another possible approach, but its applicability underwater is strongly constrained by seawater's high electrical conductivity. In practice, RF systems are mainly considered in the extremely low frequency (ELF) and low frequency (LF) ranges, where attenuation is less severe, albeit at the cost of very limited bandwidth and data rate. At higher frequencies, especially in the MHz-to-GHz range, electromagnetic waves are attenuated so strongly that the effective communication range is reduced to only a few meters [5]. As a result, RF links are generally restricted to highly localized, short-range underwater applications.

To overcome the limitations of acoustic and RF systems, UWOC technology has emerged as a highly promising solution [6]. Optical links offer several important advantages, including high bandwidth, low latency, and the potential for energy-efficient data transmission. As a result, this technology can support data rates up to the Gbps over distances of hundreds of meters, making it particularly attractive for data-intensive applications such as real-time video transmission, underwater sensor networks, and AUVs communications [7]. At the same time, underwater optical propagation is strongly affected by absorption, scattering, and water turbidity, which significantly constrain the achievable range and link reliability.

A comparative overview of underwater communication methods based on acoustic, RF, and optical waves is presented in Figure 1, while Table 1 summarizes their principal performance parameters.

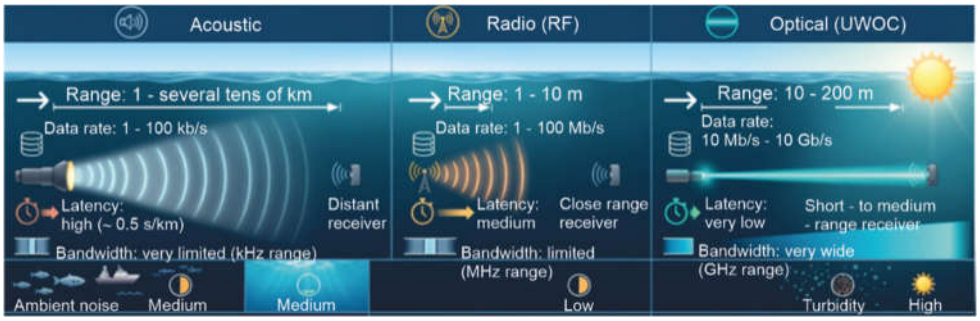

Figure 1. Comparative analysis of underwater wireless communication technologies.

Table 1. Comparison of UOWC technologies [8–11].

Parameters	Acoustic	RF	Optical
Distance	Dependent on frequency—up to several tens of km	Dependent on frequency: ~ 10 m (VHF/UHF)	10—200 m
Data rate	1 kbps—100 kbps	up to 100 Mbps	up to 10 Gbps
Attenuation	0.1—4 dB/km	3.5—5 dB/m	0.39 dB/m (ocean) 11 dB/m (turbid)
Bandwidth	(1—100) kHz distance dependent	MHz	150 MHz
Frequency	10 Hz—100 kHz	3—30 MHz	400—800 THz

 doi:10.20944/preprints202606.0076.v1

Latency	High	Moderate	Low
Environmental influence	Pressure, temperature, and salinity	Conductivity and permittivity	Absorption, scattering, turbidity

The comparison highlights the fundamental trade-offs among these technologies in terms of transmission range, data rate, latency, and sensitivity to environmental conditions. Acoustic communication offers the longest operational range, but at the expense of low throughput and high latency. RF links offer lower latency and potentially higher data rates than acoustic systems, yet their range remains severely limited due to strong attenuation in water. By contrast, optical communication supports the highest throughput and low latency, but it is sensitive to water quality. That is why these properties enable their use in many scenarios of communication systems operating in aquatic environments.

Figure 2 illustrates a networked communications for several maritime platforms, including surface ships, submarine sensor nodes (SSNs), remotely operated vehicles (ROVs), and autonomous underwater vehicles (AUVs), based on optical data links. In this concept, the surface vessel may act as a supervisory or relay platform, while underwater nodes form a multipoint sensor network enabling communication, coordination, and synchronization between autonomous vehicles and distributed sensing units. In such a configuration, UWOC can provide high-speed, low-latency links suitable for real-time video transmission, rapid sensor-data exchange, and cooperative operation of underwater platforms. However, there are several practical challenges for UWOC applications, e.g., link geometry, platform alignment, and water reservoir properties.

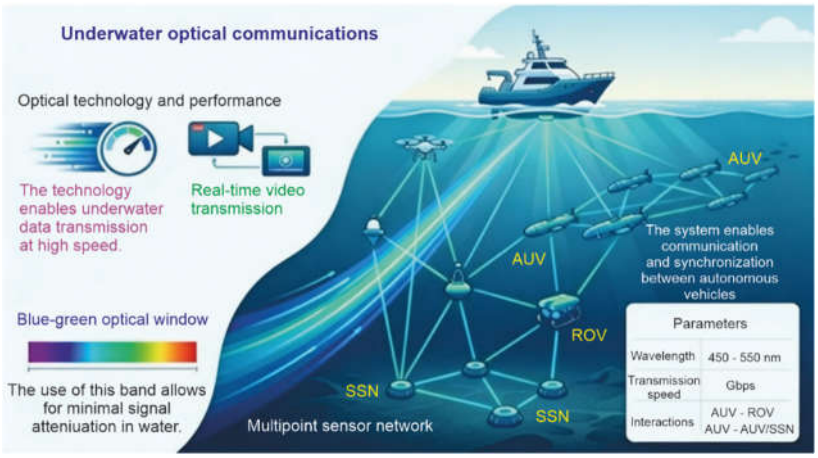

Figure 2. Generic architecture of the UWOC system showing optical links between a surface vessel, AUVs, ROVs, and SSNs. The scheme illustrates a multipoint underwater sensor network operating in the blue-green optical window to enable high-speed, low-latency communication.

2. Fundamentals of Underwater Optical Communications

UWOC systems offer high data rates, physical-layer data security, free licensing, and low installation and operating costs. However, the main drawback of UWOCs is the strong absorption and scattering of optical radiation. Fundamentally, water has low optical absorption in the blue-to-green wavelength range. However, the attenuation level depends on the kind of water reservoir. For example, the lowest absorption coefficients occur at around 420-460 nm (blue light) in seawater and at around 540-550 nm (green light) in coastal water [12,13]. As a result, blue light penetrates deepest in open-ocean seawater, while in coastal areas, green light is more effective. Absorption refers to the irreversible conversion of optical energy into heat caused by pure water molecules, phytoplankton, and dissolved organic matter [14].

Scattering occurs when particles in water deflect photons from their original path. In the UWOC links, it causes beam broadening and intersymbol interference at the receiver. In addition to

 doi:10.20944/preprints202606.0076.v1

absorption and scattering, underwater optical links are also affected by turbulence, which results from temperature and salinity variations that produce refractive-index fluctuations. These fluctuations may cause scintillation, beam wandering, and intensity fading at the receiver, thereby degrading link stability and overall communication performance.

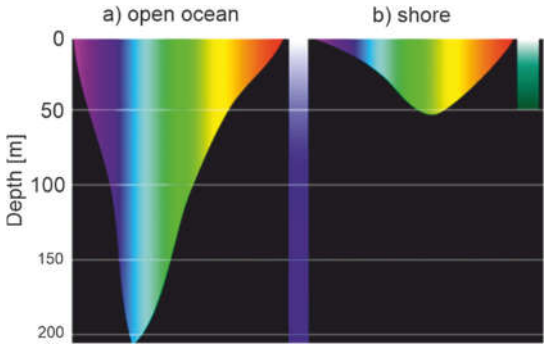

Figure 3. Penetration depth of optical radiation in seawater: a) in the open ocean, b) in coastal regions [15].

To design reliable UWOC systems, researchers must conduct comprehensive channel modeling that accounts for different water types, dynamic turbulence, and beam-steering characteristics.

Figure 4 shows a block diagram of a UWOC system. The transmitter subsystem comprises a data input fed into a modulator, a driver circuit, a light source (LED or LD), and collimating optics. The optical signal propagates through the aquatic channel, subject to absorption, scattering, and turbulence. At the receiver, the collecting optics focus the light onto the PD surface (photodiode surface). The radiation is spectrally filtered to minimize the influence of background light. The resulting PD signal (current) is amplified by an amplifier (transimpedance, TIA), then demodulated, and finally delivered as the recovered data output.

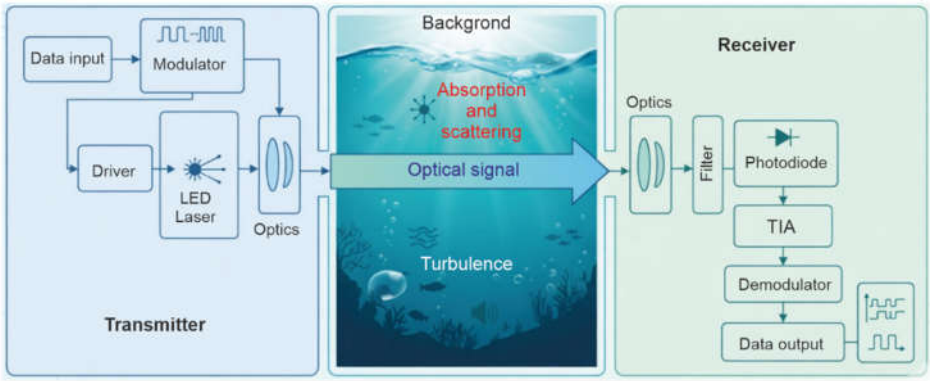

Figure 4. Schematic of a typical UWOC link.

The characteristics of the underwater optical channel (wavelength-dependent attenuation, turbulence, scattering, and link geometry) determine the required spectra and optical power of the light source, beam divergence, modulation bandwidth and format, and receiver sensitivity. Consequently, the design of UWOC requires joint optimization of the transmitter and receiver construction.

2.1. Optical Radiation Sources

The optical transmitter is one of the key subsystems determining the achievable data rate, communication range, power efficiency, and robustness of an UWOC link. It employs optical sources operating approximately between 450 and 570 nm to minimize water radiation attenuation. The two most commonly used semiconductor sources in UWOC are LEDs and LDs. These sources differ substantially in beam divergence, modulation bandwidth, spectral width, optical power density, cost,

 doi:10.20944/preprints202606.0076.v1

and alignment requirements. LEDs generally exhibit large beam divergence angles, low cost, simpler driving electronics, and higher tolerance to pointing errors. Laser diodes, by contrast, offer a much narrower beam, higher radiance, a narrower emission spectrum, and a larger modulation bandwidth, which make them more suitable for high-speed, longer-distance line-of-sight UWOC links [16].

LEDs are attractive optical transmitters for short- and medium-range UWOC systems, especially when low cost, low power consumption, mechanical simplicity, and relaxed alignment are more important than maximum data rate. Recent experiments show that LED-based UWOC can nevertheless achieve practically useful performance. Zhang and Zhou demonstrated a real-time UWOC system using four blue LEDs with pre-emphasis technology to extend the modulation bandwidth. Their system achieved a data rate of 135 Mbps at a distance of 10 m with a BER of $5.9 \cdot 10^{-3}$, and the estimated maximum communication distance was 25.4 m at 80 Mbps under the same water conditions [17]. This result is important because it concerns a real-time system, not only an offline laboratory demonstration.LED arrays and multi-emitter configurations are also relevant for UWOC. Li et al. demonstrated a MIMO-UWOC system based on arrayed LEDs, showing that spatial diversity can mitigate turbulence-induced fading and improve tolerance to misalignment [18].

Laser diodes are currently the dominant sources for high-speed UWOC links. Their low beam divergence provides longer transmission distances, and a narrow spectral width reduces the impact of background light. Oubei et al. demonstrated a 2.3 Gbit/s UWOC link over 7 m using a directly modulated 520 nm laser diode. The authors noted that the LD's high modulation bandwidth, combined with receiver sensitivity, was the key factor enabling high-speed transmission. Shen et al. reported a compact, low-power UWOC system based on a 450 nm laser diode, achieving 2 Gbit/s over 12 m and 1.5 Gbit/s over 20 m [19].

Longer-distance LD-based links have also been reported. Wang et al. demonstrated a 100 m, 500 Mbps underwater optical wireless link using a 520 nm green LD with NRZ-OOK modulation. The higher modulation bandwidth of LDs was identified as a crucial factor for implementing high-speed UWOC systems [20]. From a materials and wavelength perspective, GaN- and InGaN-based blue and green LDs are particularly important. Commonly used wavelengths include approximately 405 nm, 450 nm, 488–490 nm, and 520 nm.

In addition to conventional edge-emitting LDs, vertical-external-cavity surface-emitting lasers (VECSELs) have recently attracted attention as advanced UWOC sources. VECSELs can provide high output power, excellent beam quality, and flexible cavity design. These properties are valuable for long-distance UWOC, where beam quality and power stability directly affect the link budget.

Tian et al. demonstrated a 108 m UWOC link using a 100 mW, 490 nm blue VECSEL with an acousto-optic modulator (AOM). The system used 64-pulse position modulation (PPM) and achieved a BER of $2.7 \cdot 10^{-5}$. They also emphasized that the VECSEL's near-diffraction-limited beam quality makes the system more suitable for practical long-distance applications [16]. Table 2 summarizes and compares key parameters of LEDs and LDs used in UWOC systems.

Table 2. Key parameters of LEDs and LDs used in UWOC systems.

Feature	LED	LD
Beam divergence	Large; easier alignment	Small; higher directionality
Typical link type	Short/medium range, local networks, sensor system.	High-speed, LOS links, longer-range links, AUV/ROV communication.
Modulation bandwidth.	Usually limited; can be improved by preemphasis, simple driving electronics.	High; suitable for Mbps-Gbps transmission.
Cost and complexity	Low-cost, simple driving electronics.	Higher optical and electronic complexity.
Main advantage	Robustness to misalignment, simplicity, and low cost.	High data rate, longer range, high optical power density.

 doi:10.20944/preprints202606.0076.v1

Main limitation	Geometrical spreading, lower bandwidth.	Strict alignment, pointing/tracking requirements.

The future performance of UWOC systems depends on the development of blue–green optical sources. The most promising directions include high-power, high-bandwidth laser diodes, VECSELs with excellent beam quality, LED arrays for robust short-range communication, and multi-emitter MIMO architectures. UWOC transmitters will likely combine an optimized source considering wavelength, high modulation capability, efficient beam shaping, and possibly spatial diversity to balance data rate, range, power consumption, and alignment tolerance.

2.2. Optical Detectors

Selecting the appropriate PD is a key factor in determining the performance of a UWOC system. In an underwater environment, the PD must provide high spectral sensitivity within the water-transmission window, a fast response time, and low noise. This section discusses the five main types of PDs used in UWOC systems: photomultipliers (PMTs), p-i-n photodiodes (PINs), avalanche photodiodes (APDs), single-photon avalanche diodes (SPADs), and silicon photomultipliers (SiPMs/MPPCs). Each of these solutions has a different detection mechanism, sensitivity, and power-supply complexity.

Photomultipliers operate based on the external photoelectric effect. This effect involves the emission of electrons from the surface of a material (metal or semiconductor) in response to incident optical radiation. A photomultiplier is a vacuum device in which all components are enclosed within an evacuated envelope (Figure 5). The first element is the entrance window, whose material—borosilicate glass, synthetic silica, or magnesium fluoride—is selected according to the required spectral range.

Immediately behind the window is the photocathode, which is a thin layer of photoemissive material. The materials used—such as bialkali, multialkali, or gallium arsenide phosphide—exhibit high quantum efficiency in the visible region, and their selection determines the spectral sensitivity of the entire device. Dynodes—a series of electrodes (usually 10 to 15) made of materials characterized by a high coefficient of secondary electron emission, such as beryllium oxide, magnesium oxide, or gallium phosphide—are arranged behind the photocathode. Each dynode is maintained at a successively higher electrical potential, supplied by an external voltage divider network connected to a high-voltage source of 500–2000 V. The electrode system is terminated by an anode, which collects the multiplied electron current and delivers the output signal to an external measurement system.

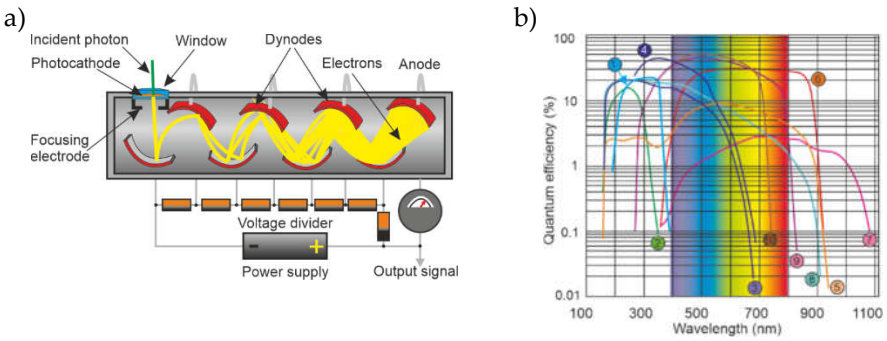

Figure 5. Schematic of a photomultiplier tube (a) [21], and spectral sensitivity curves of various photocathodes (b) [based on 22]. Curves 1–6 correspond to photocathodes with synthetic silica windows: 1—GaN, 2—CsTe, 3—bialkali, 4—ultra-bialkali, 5—enhanced-red multialkali, and 6—GaAs. Curves 7–10 correspond to photocathodes with borosilicate glass windows: 7—InGaAs, 8—multialkali (S20), 9—enhanced-red GaAsP, and 10—GaAsP.

In this construction, a photon passing through the entrance window strikes the photocathode and—if its energy is greater than the work function of the material—ejects a single photoelectron.

 doi:10.20944/preprints202606.0076.v1

The emitted electron is then accelerated by the electric field between the photocathode and the first dynode, striking the dynode surface with sufficient kinetic energy to induce secondary electron emission. Each collision with a subsequent dynode results in the emission of several secondary electrons, with the secondary emission coefficient d on a single dynode typically ranging from 3 to 6, depending on the electrode material and the applied voltage. This process cascades through all dynodes, and the total current gain $G = \eta\,(d \cdot g)n$, where n is the number of dynodes, g is the transfer efficiency between adjacent dynodes, and η is the collection efficiency between the photocathode and the first dynode (typically 0.7–0.9). For a typical PMT with n = 10 dynodes and $\delta \approx 5$, the total current gain reaches values of 10^6–10^7.Among the operational parameters, current responsivity (A/W) is particularly important, along with the dark current resulting from thermionic electron emission from the photocathode and the output pulse rise time, typically 1–3 ns, which limits the device bandwidth. The exceptionally high gain of PMTs makes them preferred PDs for applications in which the optical signal is strongly attenuated, such as long-range UWOC links or systems operating in highly scattering environments. However, the main limitations of PMTs include their relatively large size and weight, high cost, the requirement for a high-voltage power supply, and sensitivity to intense background illumination, which may cause saturation and accelerate photocathode degradation. These characteristics complicate PMT integration into compact autonomous underwater vehicle (AUV) platforms, where compact size and system reliability are critical.

Photomultipliers can operate either in linear (analog) mode, in which the anode current is proportional to the incident photon flux and enables faithful reproduction of the optical signal modulation, or in single-photon counting (SPC) mode, in which each detected photon produces a clearly distinguishable anode pulse that is registered by a discriminator and counting circuit. The latter mode is possible because the PMT gain is sufficiently high to distinguish the single-photoelectron pulse from the readout system's electronic noise.

UWOC systems also employ PDs based on the internal photoelectric effect, such as PINs and APDs. The PIN architecture is shown in Figure 6a, while the corresponding energy-band diagram is presented in Figure 6b. This structure is characterized by the insertion of an undoped semiconductor region between the p-type and n-type layers. This additional region, denoted as the intrinsic (i) layer, significantly increases the width of the depletion region, where photon absorption and electron–hole pair generation occur.

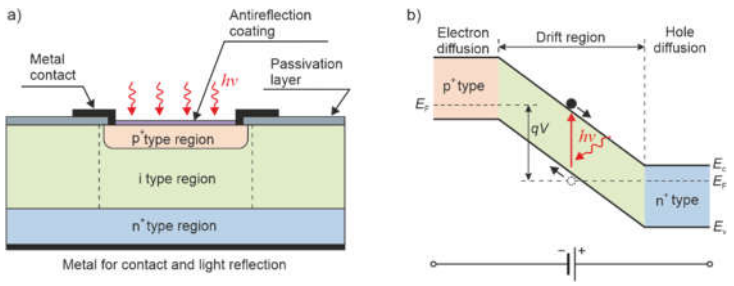

Figure 6. PIN photodiode: (a) geometry, (b) energy-band diagram at reverse bias.

The introduction of an intrinsic layer between the p- and n-regions significantly improves the PIN's key performance parameters. This layer increases the width of the depletion region, thereby enhancing the probability of photon absorption and enabling more efficient separation of photogenerated charge carriers in a strong electric field. As a result, PINs exhibit lower junction capacitance and, therefore, faster time response.

Another photodiode construction is the APD, which provides internal gain through avalanche multiplication of charge carriers. The APD structure is specifically designed to generate a strong electric field within a dedicated multiplication region. This field is sufficiently high for accelerated carriers to acquire enough kinetic energy to initiate impact ionization, leading to the generation of additional electron–hole pairs (Figure 7).

 doi:10.20944/preprints202606.0076.v1

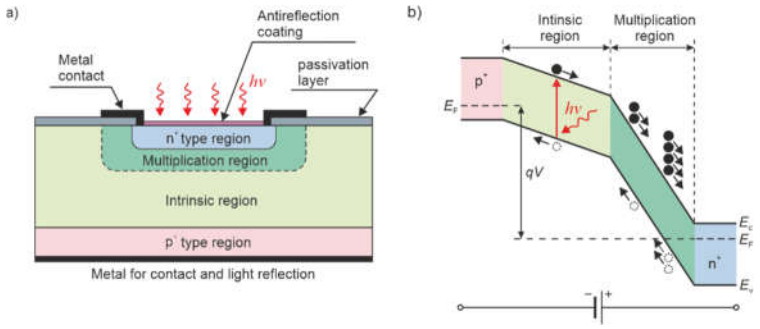

Figure 7. APDs: (a) structure, (b) energy band diagram at reverse bias.

The APD operates on the same fundamental principle as a PIN: photon absorption generates an electron–hole pair, which is subsequently separated by an electric field. Unlike conventional photodiodes, however, the APD employs an additional carrier multiplication mechanism based on impact ionization. The gain of an APD is defined as the ratio of the total photocurrent, including avalanche multiplication (I_{APD}), to the primary photocurrent (I_{ph}), which would be generated solely by photon absorption in the absence of internal amplification, and can therefore be expressed as

$$M = \frac{I_{APD}}{I_{ph}} \qquad (1)$$

In practice, the avalanche gain M depends strongly on the applied reverse bias voltage V and temperature, and can be described by the empirical relation [23]

$$M = \frac{1}{1-\left(\frac{V}{V_{br}}\right)^{\kappa}}, \qquad (2)$$

where V_{br} is the breakdown voltage, and κ is an empirical exponent that depends on the photodiode material and operating conditions. For silicon APD, values of κ in the range of 2–6 are typically reported. This relationship indicates that the avalanche gain increases nonlinearly with increasing reverse bias voltage, exhibiting a sharp rise as the breakdown voltage is approached.

To achieve avalanche multiplication, APDs require a high reverse bias voltage, typically ranging from several tens to several hundred volts, and precise control of both the bias voltage and the temperature. Compared with conventional photodiodes, APDs are more sensitive to noise, thermal effects, and nonlinear gain behavior. Despite these limitations, their ability to internally amplify the photogenerated signal at the detection stage makes them widely used in highly sensitive receiving systems.

Although linear-mode APDs significantly improve receiver sensitivity through internal avalanche multiplication, their output current remains proportional to the incident optical power. However, under extremely low-light conditions, even higher sensitivity is required, which has motivated researchers to develop PDs capable of single-photon detection.

SPADs are among the most advanced solid-state technologies for single-photon detection. They operate in Geiger mode, which enables the registration of individual photons with high sensitivity and excellent temporal resolution. In contrast to APDs operated in linear mode, SPADs do not generate an output signal proportional to the number of incident photons. Instead, each detected photon triggers a discrete electrical pulse corresponding to a single detection event. For this reason, SPADs are also commonly referred to as Geiger-mode avalanche photodiodes (G-APDs), by analogy with Geiger–Müller PDs [24], in which ionizing radiation initiates a self-sustaining avalanche process.

A typical SPAD is based on a p–n or p–i–n junction that is operated above its breakdown voltage. In Geiger mode, the applied bias voltage Vbias exceeds the breakdown voltage Vbd. The difference

$$V_{ex} = V_{bias} - V_{bd}, \qquad (3)$$

is called the excess bias voltage (or overvoltage), and it is one of the most important parameters that determines the PD's performance.

 doi:10.20944/preprints202606.0076.v1

The operation of a SPAD does not depend solely on the value of V_{ex}, but also on the junction geometry and doping profile, which together determine the electric field distribution in the multiplication region. This field controls the probability that an avalanche process will start after a photon is absorbed. The breakdown voltage varies for different SPAD technologies and can range from about 10 V to several hundred volts. As a result, the excess bias voltage typically varies from below 1 V to several tens of volts. Therefore, when designing and optimizing SPADs, it is important to focus on the electric-field distribution and the junction structure rather than solely on the absolute value of the applied voltage. When a photon is absorbed in the device's active region, it creates an electron–hole pair. In a strong electric field, this pair can trigger a rapidly growing avalanche process. The avalanche occurs locally within the depletion region, producing a large current pulse. Importantly, the amplitude of this pulse does not depend significantly on the energy of the incoming photon. Because the avalanche gain is very high, typically in the range of 10^5 to 10^7 [25], the device enables single-photon detection with high reliability and provides a very fast timing response, usually below one nanosecond.

As the excess bias voltage Vex increases, the electric field in the multiplication region becomes stronger, increasing the avalanche initiation probability. Consequently, the photon detection efficiency (PDE) increases monotonically with Vex until it approaches saturation, as the avalanche triggering probability tends toward unity. At the same time, stronger electric fields reduce statistical fluctuations in avalanche buildup time, thereby improving the PD's timing resolution. Modern silicon SPADs achieve timing jitter of a few tens of picoseconds under optimized bias conditions.

However, higher electric fields also increase the rate of spurious avalanche events not initiated by signal photons. The main sources of these events are thermally generated carriers, which dominate at room temperature, and band-to-band tunneling, which becomes significant at high electric field strengths. Together, these mechanisms determine the dark count rate (DCR). An additional noise contribution arises from afterpulsing, which is caused by charge carriers trapped in lattice defects during a preceding avalanche event and released after a characteristic trapping lifetime, often during or shortly after the recovery time.

Consequently, PDE, timing jitter, and DCR are strongly interrelated through the device's avalanche physics and noise mechanisms, giving rise to a fundamental design trade-off: increasing Vex improves detection efficiency and timing performance at the cost of increased noise. Optimizing SPAD operation, therefore, requires careful selection of the bias point, as well as engineering of the junction structure and doping profile to achieve the desired balance between sensitivity, timing accuracy, and dark count suppression.

At low reverse bias, the device operates in the unity-gain regime, where the output current equals the primary photocurrent generated by the absorbed radiation (Figure 8a). As the bias voltage increases, the device transitions into linear mode, in which internal carrier multiplication becomes significant, and the output current IAPD is given by the product of the primary photocurrent Iph and the avalanche gain M. Once the applied voltage exceeds the breakdown voltage Vbr, a suitably designed PD, such as a SPAD, can enter Geiger mode. This regime serves as the operating basis for SPADs. It is sustained by exceptionally strong electric fields within the depletion region, typically exceeding 10^5 V/cm, under which any individual electron or hole can acquire enough energy to trigger a complete avalanche multiplication event.

As shown in Figure 8b, the onset of an avalanche causes the device current to rise rapidly to a macroscopic value. This current persists until the avalanche is quenched—that is, until the bias voltage is lowered to or below Vbr, at which point the electric field becomes too weak to sustain impact ionization and the current ceases. The PD cannot register further photons until the bias is raised back above breakdown; this restoration step is known as the reset phase. Together, the quenching and reset phases are managed by dedicated electronics commonly referred to as quenching circuits.

 doi:10.20944/preprints202606.0076.v1

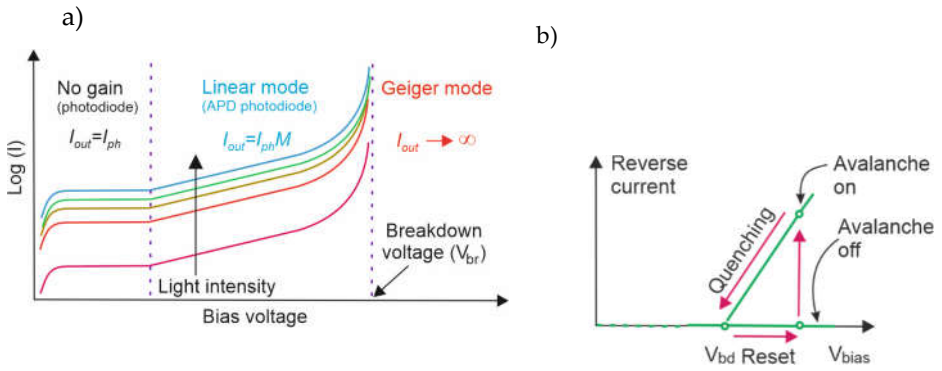

Figure 8. Reverse current as a function of reverse bias voltage in an APD [based on 26].

The function of a quenching circuit is to handle the avalanche current produced by a single-photon detection event and return the PD to its sensitive state in a controlled manner. Specifically, it must: (i) limit the avalanche current to a safe level to avoid device degradation; (ii) terminate the avalanche in a reproducible way; and (iii) restore the operating bias above breakdown to allow detection of the next photon.

Two principal categories of quenching circuits are distinguished in the literature. In passive quenching circuits (PQCs), a series resistor inserted in the bias path limits avalanche current and allows the junction voltage to drop naturally below breakdown. This approach is straightforward to implement and requires no additional active components, but the relatively slow voltage recovery inherent to an RC discharge results in comparatively long dead times [27]. Active quenching circuits (AQCs) address this limitation by incorporating fast sensing electronics that detect the onset of the avalanche and deliberately force the bias voltage below breakdown within a few nanoseconds. Once the avalanche is extinguished, the bias is actively restored, yielding substantially shorter dead times and superior timing resolution compared with passive implementations [28].

Despite its ability to detect individual photons with exceptional sensitivity, a single discrete SPAD has an important functional constraint: every detected photon initiates a self-sustaining avalanche that must be quenched and reset before the device becomes sensitive again, limiting the device to registering only one photon per detection cycle. To extend counting capability and increase the effective dynamic range, PD's architectures have been developed that monolithically integrate large numbers of SPAD microcells, ranging from several hundred to several thousand, on a single semiconductor substrate. The device's output is formed by summing the contributions of all microcells, allowing multiple simultaneous photon arrivals to be resolved. Devices of this type are known as silicon photomultipliers (SiPMs) or, using the trade name introduced by Hamamatsu, multi-pixel photon counters (MPPCs).

Two principal classes of SiPMs are commonly distinguished: analog SiPMs (aSiPMs) and digital SiPMs (dSiPMs).

In the analog SiPM architecture, all microcells are wired in parallel to a single output node (Figure 9a). Each microcell is equipped with its own integrated quenching resistor Rq, which serves a dual purpose: it ensures that each SPAD operates independently in Geiger mode, and it allows the individual cell signals to be passively combined at the common output. The resulting output waveform carries amplitude information proportional to the number of microcells fired simultaneously, enabling the device to resolve the number of detected photons on an event-by-event basis (Figure 9b), provided that each triggered cell was struck by a distinct photon within the same time window.

 doi:10.20944/preprints202606.0076.v1

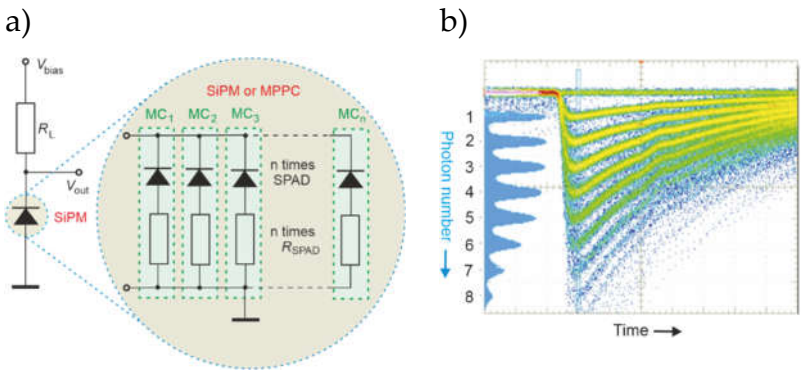

Figure 9. Electrical circuit of the SiPM (a), and output signals (b) of the MPPC module, type C-10507-11-050U, where: R_L is the SiPM load resistor, and MC is the microcell.

The characteristics described above have established aSiPMs as the PD of choice in a broad range of low-light applications operating at moderate photon fluxes. They benefit from a well-matured fabrication process, a simple circuit architecture, and an attractive balance between cost and performance. However, several intrinsic drawbacks limit their applicability in more demanding scenarios. Because all microcell signals are merged into a single analog sum, information about the arrival time of individual photons is irretrievably lost. Furthermore, the voltage swing produced by a single microcell discharge is typically no more than a few millivolts, making the output vulnerable to electronic noise and threshold instability, a problem that becomes particularly pronounced when the dark count rate is high. Signal integrity is further compromised by parasitic capacitances introduced by on-chip metal interconnects, bond wires, and the external load resistor R_L, which together cause pulse broadening, amplitude reduction, and increased timing jitter.

Although aSiPMs are adequate for applications in which the integrated photon count is the primary observable, their shortcomings become apparent whenever precise temporal information is required. The low amplitude of the single-cell output signal places demanding constraints on front-end amplifier design and necessitates careful signal conditioning to maintain an acceptable signal-to-noise ratio. Parasitic impedances distributed across the interconnect network further distort the pulse shape and introduce timing uncertainty that is difficult to compensate for at the system level. Most critically, because all microcell contributions are merged into a common analog waveform, the aSiPM cannot assign arrival times to individual photon detection events, thereby fundamentally excluding it from time-resolved measurement applications. Its use, therefore, remains confined to scenarios in which amplitude-based photon-flux estimation is sufficient.

The limitations of analog architectures have motivated the development of digital SiPM (dSiPM) designs, in which the readout is restructured at the microcell level. Rather than summing all cell outputs into a shared analog line, each SPAD microcell in a dSiPM is paired with its own dedicated readout channel comprising front-end discriminator electronics and a time-to-digital converter (TDC). This arrangement allows every photon detection event to be independently registered, counted, and assigned a precise timestamp without interference from neighboring cells.

The consequences for system performance are significant. Single-photon sensitivity is preserved, while the fully digital nature of the output eliminates the analog noise and baseline fluctuation problems that affect aSiPMs. Spatial and temporal information are available simultaneously at the pixel level, enabling applications that require both photon-number resolution and high timing accuracy. From an engineering standpoint, the digital architecture also improves noise immunity and naturally scales to large-format PD arrays [29]

The PD technologies discussed above differ fundamentally in their internal operating principles, gain mechanisms, and noise characteristics, and these differences can have a practical impact on UWOC system performance. Parameters such as sensitivity, bandwidth, dead time, dynamic range,

 doi:10.20944/preprints202606.0076.v1

and biasing complexity directly determine achievable transmission distance, supported data rate, alignment tolerance, and receiver architecture. Therefore, after examining the physical operating principles of the main PD classes, it is now necessary to analyze how these properties translate into practical UWOC implementations and into experimentally demonstrated communication systems.

3. Photodetectors' Technologies in UWOC

PMTs constitute an important class of highly sensitive PDs used in UWOC. Their high internal gain, low noise, relatively large photosensitive area, and good sensitivity in the blue–green spectral region make them attractive for long-range and low-light UWOC links, where the received signal may approach the photon-counting regime. At the same time, PMT-based receivers require careful system design due to their high-voltage operation, sensitivity to excessive illumination, dependence of the output signal characteristics on the received optical power, and practical constraints on size and cost [30].

Early experimental work demonstrated the practical usefulness of PMTs in underwater optical links. Cox developed a 405-nm laser-diode-based underwater optical communication system with a PMT receiver. The system achieved 500 kbps with return-to-zero (RZ) modulation and 1 Mbps with non-return-to-zero (NRZ) modulation in a controlled water-tank environment [29]This work is historically important because it demonstrated that PMT-based detection could be applied not only to laboratory photon-detection experiments but also to practical underwater optical data transmission.

In recent years, PMTs have been increasingly used in long-range and high-sensitivity UWOC demonstrations. Fei et al. reported a wideband UWOC system that used a 450-nm laser diode and a commercial PMT receiver to achieve 100.6 m underwater transmission at data rates up to 3 Gbps [31]. The authors also demonstrated that the PMT's relatively large effective area improved tolerance to link misalignment, particularly relevant for long-range underwater links involving moving or vibrating platforms. Thus, in this system, the PMT enabled a combination of long transmission distance, gigabit-class data rate, and relaxed alignment requirements.

A major issue in PMT-based UWOC receivers is that the PMT output waveform is highly dependent on the received optical power. At extremely weak powers, the output consists of discrete pulses corresponding to individual photoelectron events. As the optical power increases, the pulse density rises, leading to significant pulse overlap; eventually, the output evolves into a continuous waveform [32]. This behavior effectively defines three operating regimes of the PMT: photon-counting (low power), transition (medium power), and quasi-continuous (high power). This regime-dependent signal formation directly impacts the choice of detection methods. Conventional detection approaches are typically designed for a single statistical model and therefore operate effectively only within a specific regime.

Liu et al. proposed detection methods based on the generalized extreme value (GEV) distribution that provide accurate performance across all three regimes [33]. These methods were shown to outperform conventional Poisson- and Gaussian-based maximum-likelihood PDs under varying received optical powers, data rates, sampling rates, and background optical conditions [34]. This issue is particularly important in practical UWOC systems, where the channel is highly dynamic, and the received signal power may vary over several orders of magnitude due to, e.g., attenuation, turbulence, beam wander, terminal vibration, and changes in link distance.

Another important tool is the use of analog-mode PMTs for weak-signal detection. Ge et al. proposed a new method for detecting weak optical signals in UWOC systems. Their system used an analog-mode PMT and on-off keying (OOK) as the modulation scheme [34]. The main challenge they addressed was pulse overlap. When the received light is very weak, the PMT generates short electrical pulses in response to individual photons. As more photons arrive, these pulses start to overlap, making it difficult for conventional methods to count them correctly. Traditional approaches either count pulse peaks or measure signal amplitude, both of which become unreliable when pulses overlap. To solve this problem, the authors proposed the pulse width counting (PWC) method.

 doi:10.20944/preprints202606.0076.v1

Instead of counting the number of pulses, they measured how long the signal remained above a fixed threshold. The key advantage is that when two pulses start to overlap, the total pulse width decreases gradually and smoothly, whereas the number of detected peaks drops suddenly from two to one. This sudden drop causes counting errors in peak-based methods, whereas the PWC method avoids this problem because it relies on a continuously changing quantity. They tested the system in a 7-meter water tank and achieved a data rate of 10 Mbps with a sensitivity of −71.5 dBm, meaning the system could work correctly even with an extremely weak received signal. Compared to the conventional methods, the PWC method required 1.1 dB less optical power than pulse peak counting and 3.8 dB less than pulse amplitude detection—the lower the required power, the better the system performance. Their results show that analog-mode PMT PDs can be used to build highly sensitive UWOC receivers, provided the signal-detection algorithm accounts for the PMT's behavior under low-light conditions, particularly the tendency for pulses to overlap at higher photon arrival rates.

PMTs are also relevant to photon-counting UWOC architectures, especially when receiver sensitivity and photon efficiency are critical. Photon-counting reception is naturally compatible with pulse-position modulation, because information is encoded in the temporal position of photon arrivals rather than only in signal amplitude. For example, photon-counting UWOC systems using PPM have demonstrated very high photon efficiency and operation under extremely low received signal levels [35]. Such results indicate that photon-counting reception, including PMT-based implementations, can be useful for long-range links, highly attenuating water channels, and applications with severely limited optical power budgets.

PMT arrays have also been investigated for MIMO-UWOC and spatial-diversity reception. In such systems, several PMTs can be used to increase the effective collection area, relax pointing requirements, or support spatially distributed signal acquisition. Li et al. proposed photon-counting schemes for MIMO UWOC with arrayed PMTs, which are relevant for long-range links and systems operating under low photon flux [36]. This approach is particularly attractive in underwater environments because spatial diversity can mitigate fading, misalignment, and local fluctuations in received intensity caused by scattering or turbulence.

In summary, PMTs have been applied in UWOC receivers in three main roles: as wideband analog PDs for high-speed links, as photon-counting receivers for ultra-sensitive low-photon-flux communication, and as large-area single PDSs or PD's arrays for improved alignment tolerance and spatial diversity. Recent demonstrations show that PMT-based UWOC can reach gigabit-per-second data rates over approximately 100 m, while PMT-based photon-counting architectures can provide very high receiver sensitivity at lower data rates. The main research challenges are related to adaptive signal detection across pulse transition waveform regimes, mitigation of ambient-light and scattering-induced noise, dynamic gain control, protection against excessive illumination, and the practical implementation of compact, robust PMT-based receiver modules.

Although PIN photodiodes are widely used in optical communication systems due to their simplicity and low cost, their sensitivity is often insufficient for long-range UWOC links, where the received optical power is extremely low. Compared with PMT-based receivers, PIN-based receivers are generally more compact, easier to integrate with standard analog front-end electronics, and less complex to implement. Nevertheless, they remain highly attractive for short-range and high-speed UWOC systems owing to their fast response, good linearity, low biasing requirements, and compatibility with TIA-based receiver architectures. However, the overall performance of UWOC depends on more than just the photodiode itself. It is jointly determined by photodiode parameters such as responsivity, active area, junction capacitance, 3 dB bandwidth, and dark current, as well as by the noise and bandwidth of the front end, the optical field of view, the modulation format, the equalization method, and the underwater channel conditions, including absorption, scattering, turbidity, turbulence, and alignment stability [37].

Experimental studies confirm that PINs can be used with both laser-diode and LED transmitters. For example, Wang et al. demonstrated a UWOC system using a 450-nm laser diode, FPGA-implemented quadrature amplitude modulation (16-QAM), and a 150-MHz PIN-based receiver. The

 doi:10.20944/preprints202606.0076.v1

system achieved a data rate of 50 Mb/s over a 3 m underwater path, demonstrating that relatively simple based-PIN receivers can support digitally modulated UWOC links at moderate link distances and channel losses [38].

PINs can also be employed in receiver diversity architectures, where multiple detector elements capture the same optical signal across different spatial paths to improve robustness against channel fluctuations and extend spatial coverage. For example, Li et al. demonstrated an underwater visible-light communication system using a blue LED transmitter and an integrated PIN array [39]. The signals from all elements were combined with equal weights (equal-gain combining), effectively increasing the receiving area and improving tolerance to beam displacement. Using quadrature amplitude modulation with discrete multitone modulation (QAM-DMT), their system achieved data rates above 1 Gb/s after 1.2 m of underwater transmission, with improved alignment tolerance and spatial coverage.

Other studies have applied multi-PIN reception with maximum-ratio combining, in which signals from different receiving branches are weighted by their quality before combining. Such methods can reduce the influence of misalignment, nonuniform irradiance, fading, and scintillation in LED-based UWOC links [40]. High-speed experiments further demonstrate the potential of PIN photodiode receivers when they are combined with advanced modulation and digital signal processing.

Fei et al. reported a high-speed UWOC link using a single 450-nm laser diode and a PIN receiver [41]. The transmitted data were split into many parallel streams and sent over multiple frequency subchannels using DMT modulation. With this approach, data rates of 16.6 Gb/s over 5 m, 13.2 Gb/s over 35 m, and 6.6 Gb/s over 55 m were achieved in tap water. These results show that multi-Gb/s based-PIN UWOC links are possible when PD bandwidth, transmitter modulation bandwidth, optical alignment, water attenuation, and digital equalization are jointly optimized.

To increase sensitivity and extend the range of optical links, especially at very low received signal power levels, APDs are used in UWOC systems. The majority of high-speed UWOC demonstrations have relied on linear-mode APDs.

These PDs were employed in several experiments: Oubei et al. demonstrated 2.3 Gbit/s OOK-NRZ transmission over 7 m using a 520 nm laser diode [7], while Shen et al. extended the link to 20 m at 1.5 Gbps using a 450 nm laser [19]. Liu et al. pushed the transmission distance to 34.5 m at 2.70 Gbps using a green LD with NRZ-OOK modulation and Thorlabs APD210 PD [42].

The sensitivity advantage of linear-mode APDs becomes particularly evident at longer distances. Lyu et al. demonstrated a 42 m UWOC link using spread spectrum technology with an APD210 photodiode, achieving a receiver sensitivity of −30.5 dBm at the forward error correction (FEC) threshold [43]. Zhang and Zhou demonstrated a real-time LED-based UWOC system that achieved 135 Mbps at 10 m using a Hamamatsu S8664-30K APD, in which the large photosensitive area was selected to facilitate receiver alignment at the cost of increased junction capacitance (22 pF) [17].

Another important class of PDs used in UWOC is based on single-photon avalanche diodes. In photon-starved conditions, the SPAD receiver no longer measures a continuous photocurrent in the usual analog sense, but rather counts discrete photon-detection events. This makes it suitable for long-distance, low-power, and Internet-of-Underwater-Things (IoUT) applications, where high sensitivity may be more important than very high analog bandwidth [44].

However, after each detected photon, the SPAD must wait a period before it becomes insensitive to further photons. At higher photon fluxes, a short recovery period (dead time) in this PD leads to a nonlinear response and limits the maximum achievable count rate. In practice, if the dead time becomes comparable to the symbol duration, missed photons may cause intersymbol interference [45]

Early SPAD-based UWOC concepts mainly used simple binary modulation formats, such as on–off keying (OOK) or pulse-position modulation, because these formats are naturally compatible with photon counting. In a simple OOK receiver, the system decides whether a “0” or “1” was transmitted

 doi:10.20944/preprints202606.0076.v1

by comparing the number of detected photons in a time slot with a threshold. In turbulent underwater channels, however, the received optical power fluctuates, so the optimum decision threshold may change with time. For this reason, studies comparing OOK and binary PPM have shown that OOK with an optimum threshold can perform slightly better, but binary PPM may be more practical when the channel state is difficult to estimate accurately [46].

An important practical issue in photon-counting UWOC is clock and data recovery. Since the SPAD output is not a smooth analog waveform but a random sequence of narrow electrical pulses, the receiver must determine the correct time slots to recover the transmitted data. Yan et al. proposed a method for directly recovering clock and data from discrete photon pulses generated by a SPAD receiver. Their experiment showed that, with an average of only 10 photons per time slot, a photon-counting UWOC system could achieve a baud rate of 1 Mbps with a BER of $3.51 \cdot 10^{-4}$. This result shows that SPAD receivers can support reliable underwater communication even when the received signal comprises only a few photons [47].

More recent work has also introduced signal-processing and machine-learning methods to improve SPAD-based UWOC receivers. Yang et al. proposed a deep learning-based method for recovering the time-slot synchronization clock from the discrete single-photon pulse sequence produced by an SPAD. In this approach, a neural network learns the hidden timing information in random photon pulses and uses it to reconstruct the clock required for data recovery. Their experimental results showed that, with an average of eight photons per time slot, a 1 Mbps photon-counting UWOC link could achieve a BER of $5.35 \cdot 10^{-4}$. This example shows that advanced digital processing can help overcome some of the practical difficulties of photon-counting reception [48].

A particularly interesting development is the use of a single SPAD receiver with orthogonal frequency-division multiplexing (OFDM) modulation. Traditionally, high-order modulation has been considered difficult for a single SPAD because the PD produces only photon-counting pulses and is strongly affected by dead time. However, Lyu et al. demonstrated that, by summing photon counts over appropriate time intervals and using OFDM signal processing, a single SPAD receiver can detect QPSK-OFDM (quadrature phase shift keying, QPSK) and 16-QAM-OFDM (quadrature amplitude modulation, QAM) signals in a UWOC experiment. The reported receiver sensitivities were as high as −84.5 dBm for QPSK-OFDM and −77.8 dBm for 16-QAM-OFDM, corresponding to fewer than 68 and 390 photons per symbol, respectively. This indicates that single-SPAD receivers can offer a compact, highly sensitive alternative to SPAD arrays in certain long-distance UWOC and IoUT scenarios.

It should be noted that the works discussed above primarily concern single-SPAD receivers, whereas SPAD arrays—such as SiPM/MPPC devices—follow a different detection paradigm. In an MPPC, a large number of SPAD microcells are connected in parallel. However, each pixel exhibits a nonlinear response governed by its individual dead time; the statistically averaged aggregate output approximates a quasi-linear PD over a practical operating range. This property makes MPPC receivers well-suited to spectrally efficient modulation formats such as OFDM with high-order QAM subcarriers. Moreover, the parallel nature of OFDM increases the effective symbol duration, further alleviating dead-time constraints, while the use of high-order QAM subcarriers improves spectral efficiency. In addition, the high sensitivity of MPPC receivers enables operation at extremely low light levels, relaxing the pointing and alignment requirements of UWOC links and enabling reliable communication even when the optical source operates close to the spontaneous-emission regime [45,49].

Beyond supporting advanced modulation formats, MPPC-based receivers enable the use of low-cost optical sources. Their high sensitivity, combined with energy-efficient schemes such as pulse-position modulation, enables reliable operation at very low received optical power levels, making them attractive for long-range UWOC systems. For example, transmission distances of 50 m and 100 m were experimentally demonstrated at data rates of 16.78 Mb/s and 8.39 Mb/s, respectively, in a standard 50-m swimming pool [50].

 doi:10.20944/preprints202606.0076.v1

Real-time implementations have also been reported: a duplex UWOC system operating in the same pool environment employed blue and green light sources together with high-sensitivity MPPC PDs, using 4-QAM OFDM modulation and convolutional coding implemented on a Field-Programmable Gate Array (FPGA) platform [51]. Despite these advances, a key limitation of MPPC receivers remains their relatively narrow bandwidth, typically on the order of a few MHz (≈4 MHz), which necessitates the use of multi-carrier modulation or advanced digital signal processing to achieve higher effective data rates [52].

The experimental studies discussed above demonstrate that the achievable performance of UWOC systems depends strongly on the selected PD's technology, modulation format, transmitter power, and propagation distance. Because the reported results span very different operating regimes, a comparative summary is useful for identifying the main system-level trade-offs.

Table 3 provides an overview of UWOC systems, illustrating the trade-off between transmission distance and achievable data rate for different PD's technologies and modulation schemes.

Table 3. Comparison of transmission distance and achievable data rates in recent UWOC systems.

Transmitter			PD	Distance [m]	Data rate	Literature
Wavelength [nm]	Power [mW]	Modulation				
LD—450	14.99	OOK	PMT	100.6	3 Gbps	[31]
LD—450	293.1	PAM-4	PMT	150	500 Mbps	[53]
LD—450	~288	PAM-4	PMT	200	500 Mbps	[54]
LED—457	N/A	PAM-8	PIN	1.2	1.5 Gbps	[55]
Blue LED	N/A	64 QAM-CAP	PIN	1.2	3.2 Gbps	[56]
VCSEL–680 [a)]	3	NRZ-OOK	PIN	5	25 Gbps	[57]
LD—520	19.4	NRZ-OOK	PIN /APD	20.7/34.5	3.48/2.7 Gbps	[42]
LD—450	10	NRZ-OOK	APD	42	1/1.9 Gbps	[43]
LD—452	12.8	DMT	APD	55	5.6 Gbps	[58]
LD—520	1400	OOK	APD	100	100 Mbps	[59]]
LD—520	N/A	NRZ-OOK	APD	100	500 Mbps	[20]
LD—450	0.5	16 QAM-OFDM	SPAD [b]	7	42.4 kbps	[44]
LED—532	1000	OOK	SPAD [b]	230-280	10 Mbps	[46][c)]
LD—452	26.2 W	OOK	SiPM	250	1 Gbps	[60]
LD—520	15	32 QAM OFDM	MPPC	21	312 Mbps	[45]
LD—450	0.174	PPM	MPPC	46	2.5 Mbps	[52]
LD—450	2400	NRZ-OOK	MPPC	100	8.4 Mbps	[50]

a) Although the 450–520 nm range represents the preferred operating window for most water types, the 680 nm VCSEL result in Table 1 highlights that highly turbid environments may favor longer wavelengths where scattering losses are comparatively reduced.
b) single SPAD.
c) theoretical analysis.

MPPC is Hamamatsu's trade name for silicon photomultipliers (SiPMs). Both terms refer to arrays of Geiger-mode avalanche photodiode microcells connected in parallel, where each microcell operates as an independent single-photon avalanche detector. Therefore, MPPC should not be treated as a separate PD's class, but rather as a manufacturer-specific implementation of the SiPM concept.

The choice of PD's technology fundamentally governs the trade-off between transmission distance and achievable data rate in UWOC systems. PIN-based receivers achieve the highest transmission speeds but have the lowest sensitivity, resulting in the shortest link ranges. Using PDs with higher sensitivity—PMT, APD, SPAD, and SiPM—enables transmission distances exceeding 100 m, though often at the cost of lower data rates. A clear inverse relationship between distance and data

 doi:10.20944/preprints202606.0076.v1

rate is observed across all PD types. Figure 10 presents a more general detector-level comparison of the achievable sensitivity and data rate ranges for the main photoreceiver technologies.

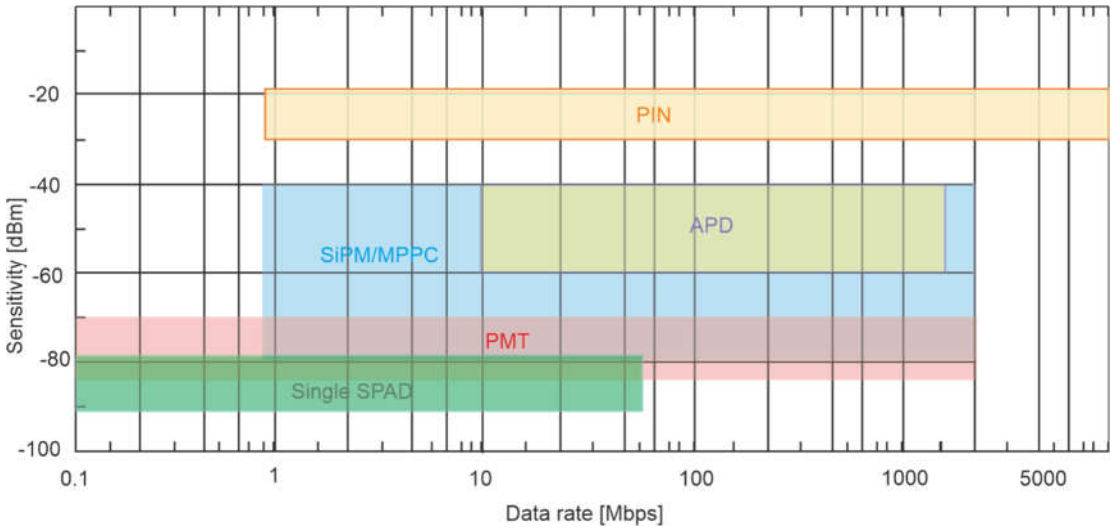

Figure 10. Comparison of receiver sensitivity and supported data rate ranges for PINs, APDs, SiPM/MPPC arrays, single SPADs, and PMTs employed in UWOC systems.

The reasons for these system-level observations become obvious when we directly analyze the internal characteristics of each PD technology. As shown in Figure 10, the PDs are clearly classified by sensitivity: single-chip SPAD PDs achieve a level between (-90 dBm and -80 dBm), followed by PMTs (-85 and -70 dBm), SiPM/MPPC arrays (-80 dBm and -60 dBm), APDs around (-60 dBm and -40 dBm), and p-i-n photodiodes around (-30 dBm and -20 dBm).

However, this sensitivity advantage comes at the cost of the supported data rate range: PINs cover the widest bandwidth, extending to several Gbps, while single SPADs are limited to approximately 50 Mbps. PMTs, despite their high sensitivity, extend to Gbps-level data rates but remain impractical for many deployments due to their physical bulk and high operating voltage. SiPM/MPPC arrays emerge as the most promising compromise, offering sensitivity far exceeding that of APDs while supporting data rates up to several Gbps. It should be noted, however, that Gbps-level data rates with SiPM/MPPC receivers have so far been demonstrated only under exceptional conditions — specifically, using a high-power transmitter formed by beam-combining eight cascaded laser diodes with a total output power exceeding 26 W, combined with a nonlinear artificial neural network-based equalizer. Under typical operating conditions, the achievable data rate of SiPM/MPPC-based receivers typically ranges from tens to hundreds of Mbps, as summarized in Table 3. It is noted that the choice of receiver technology must be carefully matched to the specific distance, data rate, and power budget requirements of the target UWOC application.

4. Other Photodetectors

The conventional photodetector technologies discussed above represent mature solutions widely deployed in UWOC systems. However, growing demands for miniaturization, underwater environmental robustness, and cost reduction are driving intensive research into emerging photodetector classes that may complement or replace conventional technologies in specific deployment scenarios. The following subsection presents selected materials and detector concepts currently under investigation, including perovskite-based structures, SiC photoelectrochemical photodetectors, and solutions tailored for Internet of Underwater Things (IoUT) applications.

4.1. Perovskite PDs

 doi:10.20944/preprints202606.0076.v1

CsPbBr3 perovskites are promising candidates for optical detectors in UWOC systems because of their spectral response (bandgap about 2.3 eV) that exactly matches the transmission window of seawater, high absorption rate, and high carrier mobility [61]. Their applications have been presented in many publications [62–64]. For example, a CsPbBr3 PD with a rise time of 82 ns, a fall time of 710 ns, a noise level of $4.3\times10^{-14}AHz^{-1/2}$, and a responsivity of 0.317 A/W was described [65].

Compared to a commercial silicon PD, perovskite provides better signal stability due to its low susceptibility to ambient light interference and also produces lower background noise. However, at higher data rates, BER degrades due to the long fall time. Therefore, reducing this time and implementing advanced coding methods will help further improve the performance of perovskite PD-based UWOC systems.

4.2. Halide Perovskite PDs

Two-dimensional halide perovskite-based PDs with broadband response, intrinsic water resistance, and high detectivity have also been developed. These characteristics are crucial for building the UWOC receiver. By matching the structure's dimensions and compositions, a broadband spectral response covering the water transmission window (>1.55 eV) can be achieved. In addition, these PDs provide a high responsivity of 3.27 A/W, a peak external quantum efficiency of 630%, fast signal rise and fall times of 0.35 ms/0.54 ms, and a high detectivity of up to 1.35×10^{12} Jones [64]

4.3. SiC-Based Photoelectrochemical PDs

In recent years, there has been a significant increase in interest in photoelectrochemical PEC PD's technologies, which enable real-time operation in the aquatic environment [66]. Additionally, the obtained spectral responsivity minimizes the impact of solar radiation, providing selective detection of ultraviolet radiation. PEC PDs do not require a power supply, which is important for their operation in aquatic environments [67]. However, the use of these devices remains a significant challenge. For example, the currently developed SiC-based PEC PDs enable operation in the ultraviolet range (375 nm) with rise/fall times of 86.5/170.95 ms, responsivity of 1244.95 mA/W, detectivity of 6.35×10^{11} Jones, and quantum efficiency of 412.45% [68]. In addition, they exhibit wide pH tolerance and high long-term operational stability in full aquatic environments.

4.4. Photodetectors for IoUT

The development of radiation sources has enabled transmission rates of up to Gbps in underwater environments, making the IoUT increasingly important [69]. High-sensitivity PDs such as PMT [70], SPAD [71], SiPM [72], and MPPC [52] were used for long-distance communication. APDs offer high sensitivity, but their noise levels significantly limit the ability to achieve a high SNR. A multi-pixel photon counter with a large active area enables efficient photon counting. By using digital techniques, significant filtering of interference and background noise can be achieved. The UWOC system, which uses MPPC operating at 5 MHz, is described in [49]. However, an important practical limitation is its high cost. The PMT also has high sensitivity, allowing the UWOC to work over long distances. However, expensive PMT operates in the short-range spectrum. Sometimes, its sensitivity is so high that it can cause damage when used at close range or in strong background light. The PMT's weight and sizes also limit its integration into a compact IoUT system for ROV or AUV platforms.

Nowadays, a high modulation bandwidth is achieved in the UWOC receiver with PDs only a few square millimeters in size, and it is the main limit for IoUT technology development. Challenging conditions in underwater environments, Pointing-Acquisition-Tracking units, and the need to provide connectivity among a large number of IoUT devices, including mobile ones, have driven the development of large-area PDs capable of high modulation rates. However, for PDs (APD arrays, PMTs, MPPCs) operating at high gain (at the level of single photons), saturation effects can be observed during changing operating conditions, e.g., working at short distances, changes in background radiation, or the use of transmitters with a large power discrepancy in the network.

 doi:10.20944/preprints202606.0076.v1

Therefore, work is still underway to implement an IoUT system with high availability and reliability [73–78].

For this purpose, scintillation optical fibers are being developed. These fibers absorb incident light and re-emit it at a longer wavelength [79,80]. The emitted light then propagates through the fiber's core to the other end. The first application of scintillation fibers for free-space optics (FSO) was reported in [81]. The advantage of this technology is, among others, the flexibility to create large-area PDs of different sizes with fast response. These devices may be a cost- and time-competitive technology compared to currently developed high-format and high-speed PDs [82–85]. In practice, this will be an important element in the construction of optical communication systems in the Non-Line-of-Sight (NLOS) configuration, significantly reducing the requirements for PAT units. A design of a large-area photoreceiver, up to several tens of cm^2, based on ultraviolet (UV)-on-blue plastic scintillating optical fibers, providing a modulation band of 86.13 MHz, was described in [74]. A laboratory UWOC setup operating at 375 nm was developed, with a distance of 1.15 m, achieving a data transmission rate of 250 Mbps at a BER of $2.2 \cdot 10^{-3}$ and NRZ-OOK encoding.

In the field of high-format PDs, important research on PV cells is also being carried out for their use in UWOC [86–90]. In practice, a PV cell can generate energy from incident light and detect variable signals emitted by UWOC's transmitter. Most previous work on PV cell-based OWC has focused on improving data throughput by using various novel PV cells. In [86], signals at 34.2 Mbit/s were received using organic PV cells and a red laser in an FSO's path of 1 m. In addition to using visible-light sources and Si-based PV cells for UWOCs [86,87,90] researchers also tested near-infrared laser and PV GaAs cells for efficient energy harvesting and high-speed FSO [91]. However, achieving long distances and high speeds requires strict geometric constraints that limit the use of conventional UWOCs on mobile underwater platforms. As a consequence, there remains a lack of work addressing these problems. Inspired by this earlier research, PV cells with dual signal acquisition and energy-harvesting functions offer good prospects for use in energy-intensive marine environments.

In [92], a prototype of the UWOC system called AquaE-lite, consisting of thin-film a-Si solar cells capable of detecting radiation at 1 $\mu W/cm^2$, was described. In a 15 m air channel, a transmission speed of 1.2 Mbps was achieved for OFDM signals at an illumination level of 109.54 lx. At a distance of 20 m, the illumination was reduced to 79.95 lux, yet data transmission at 1 Mbps was still enabled with a panel signal band of 290 kHz. OFDM signals with a bandwidth of 908.2 kbps were also obtained for a 2.4 m-long optical path through turbid water operating in direct sunlight.

5. Commercial UWOC Systems

The transition of UWOC technology from laboratory demonstrations to commercially ready products is ongoing, but the number of companies producing such systems remains limited. The following section discusses representative products that illustrate the current state of commercial UWOC technology.

Sonardyne (UK) offers the BlueComm 200 UV, an underwater optical communications and data-transfer modem designed for operation to depths of up to 4000 m. The system employs an LED array transmitter operating at a peak wavelength of 450 nm with a total optical power of 6 W, and uses a PMT in the receiver to achieve the high sensitivity required for long-range operation in low-ambient-light conditions (Figure 11).

 doi:10.20944/preprints202606.0076.v1

Figure 11. Photograph of a commercial BlueCommTM 200 system [93].

The receiver provides a 180° hemispherical field of view, which substantially relaxes pointing and alignment requirements compared with narrow-beam laser-based systems. Data rates of up to 12.5 Mb/s are supported over ranges of up to 150 m. Due to the PMT's sensitivity to electromagnetic interference, the transmitter and receiver modules are housed in separate pressure housings. The BlueComm 200 UV is targeted at subsea infrastructure inspection, ROV and AUV operations, and data harvesting in deep-water environments where acoustic links are bandwidth-limited.

Lumasys, Inc. (Woods Hole, MA, USA) develops high-bandwidth, low-power underwater optical communication systems based on LED blue-light transmission. Their optical modem product enables omnidirectional transmission and reception of optical signals over approximately 100 m at data rates exceeding 1 Mbit/s and supports underwater communication networks in which multiple modems communicate with one another. Stated system capabilities include data rates up to 20 Mb/s, a range of up to 200 m, suitability for both shallow and deep-water applications, and an integrated long-range acoustic communications and positioning unit [94]. The system is aimed at high-speed data harvesting from seabed observatories, tetherless ROV and AUV control, and live video streaming from remote subsea cameras.

Hydromea (Switzerland) offers the LUMA™ family of wireless underwater optical modems, designed for subsea data flow to enable real-time underwater communication in asset integrity and marine science missions. The LUMA™ X variant is rated for operation to depths of up to 6000 m, supports data rates of up to 10 Mb/s, and achieves a range of up to 50 m. The system is designed to be compact and energy-efficient, making it well-suited for integration with AUVs, ROVs, and distributed seabed sensor networks. The wide field of view of the optical transceiver head reduces sensitivity to platform motion and misalignment, which is a key practical consideration in dynamic underwater deployments [95].

The commercial systems surveyed above illustrate several important trends. PMT-based receivers remain the technology of choice for long-range, sensitivity-critical applications at moderate data rates, as evidenced by the BlueComm 200 UV. LED-based omnidirectional architectures, as implemented by Lumasys and Hydromea, offer practical advantages in alignment tolerance and system integration at the cost of reduced range and data rate relative to laser-based designs. The Kyocera development program demonstrates that laser-diode-based systems operating at GaN blue wavelengths are approaching Gbps-class performance in real offshore environments, pointing toward a near-term convergence between laboratory-demonstrated data rates and field-deployable system capabilities.

6. Conclusion

This paper has reviewed the principal hardware subsystems of UWOC systems, focusing on the receiver PDs that jointly determine system performance in terms of data rate, transmission distance, receiver sensitivity, and practical feasibility.

The five PD's technologies reviewed span a wide range of sensitivities and bandwidths. PINs offer the highest bandwidth and the simplest implementation, but their lack of internal gain limits their utility to short-range, high-power links. APDs extend the sensitivity by one to two orders of magnitude through avalanche multiplication, enabling links up to approximately 100 m at multi-Gbps rates. PMTs provide the highest gain among the technologies reviewed and have been demonstrated in UWOC links reaching 200 m at 500 Mbps; however, their high-voltage requirements, physical bulk, and susceptibility to saturation limit their applicability on compact autonomous platforms. SPADs operated in Geiger mode achieve receiver sensitivities approaching −85 dBm, making them attractive for photon-starved long-range links, but their inherent dead time constrains the maximum count rate and requires careful adaptation of modulation formats and signal-processing strategies. SiPM/MPPC arrays, composed of large numbers of parallel SPAD microcells,

 doi:10.20944/preprints202606.0076.v1

combine near-photon-counting sensitivity with advanced modulation formats and low operating voltage, and have been experimentally demonstrated at distances up to 250 m.

The comparative analysis of reported experimental results reveals a consistent inverse relationship between achievable data rate and transmission distance across all PD's technologies. This trade-off is not merely a consequence of channel attenuation but also reflects fundamental PD's properties, including bandwidth, sensitivity, linearity, and noise characteristics. No single detector technology simultaneously satisfies all system requirements, and the choice of receiver must therefore be co-optimized with the transmitter, modulation format, link geometry, water type, and target application.

Several directions emerge as particularly promising for future research. The integration of SiPM/MPPC PDs with advanced multi-carrier modulation, digital pre-distortion, and machine-learning-based equalization may enable simultaneous high sensitivity and high spectral efficiency. The development of compact, low-voltage photon-counting receivers based on CMOS-integrated SPAD arrays is relevant for miniaturized AUV and IoUT applications. Adaptive receiver architectures capable of operating across the photon-counting, transition, and analog regimes — such as those based on generalized statistical detection methods — address the challenge of widely varying received power levels in dynamic underwater channels.

Beyond established semiconductor technologies, emerging approaches such as perovskite photodetectors, self-powered SiC photoelectrochemical devices, and scintillating-fiber-based large-area receivers represent promising research directions that may address the specific constraints of underwater and IoUT environments, including water resistance, energy autonomy, and wide field-of-view detection.

Author Contributions: methodology Z.B., validation Z.B and JM; formal analysis Z.B and JM; investigation JM; data curation Z.B and JM; writing—original draft Z.B and JM; writing—review and editing Z.B and JM; visualization Z.B and JM; supervision Z.B. All authors have read and agreed to the published version of the manuscript.

Institutional Review Board Statement: Not applicable.

Data Availability Statement: The data presented in this study are available upon request from the corresponding author.

Informed Consent Statement: Not applicable.

Acknowledgments: During the preparation of this manuscript, the author(s) used [ChatGPT in auto mode, model GPT-4o and Google (gemini) nano banana] for the purposes of [to draw only the background for Figures: 1, 2, and 4]. The authors have reviewed and edited the output and take full responsibility for the content of this publication.

Conflicts of Interest: The authors declare no conflicts of interest. .

References

1. Kaushal, H.**;** Kaddoum, G. Underwater optical wireless communication. *IEEE Access* **2016**, *4*, 1518–1547.
2. Spagnolo, G.S.**;** Cozzella, L.; Leccese, F. Underwater optical wireless communications: Overview. *Sensors* **2020**, *20*(8), 2261.
3. Chang, Y. **A** comprehensive review of underwater optical, acoustic, and electromagnetic communication. In *Proceedings of the 3rd International Conference on Software Engineering and Machine Learning*; 2025.
4. Saeed, N.; Celik, A.; Al-Naffouri, T.Y.; Alouini, M.S. Underwater optical wireless communications, networking, and localization: A survey. Ad Hoc *Netw.* **2019**, *94*, 101935.
5. Che, X.**;** Wells, I.; Dickers, I.; Kear, G.; Gong, P. Re-evaluation of RF electromagnetic communication in underwater sensor networks. *IEEE Commun. Mag.* **2010**, *48*, 143–151.

 doi:10.20944/preprints202606.0076.v1

6. Joseph, L.; Anandan, S. A review on feasible and reliable underwater wireless optical communication system for achieving high data rate and longer transmission distance. *Int. J. Electron. Telecommun.* **2022**, *68*(4), 815–823.
7. Oubei, H.M.; Li, C.; Park, K.H.; Ng, T.K.; Alouini, M.S.; Ooi, B.S. 2.3 Gbit/s underwater wireless optical communications using directly modulated 520 nm laser diode. *Opt. Express* **2015**, *23*(16), 20743–20748.
8. Huang, J.; Diamant, R. Adaptive modulation for long-range underwater acoustic communication. *IEEE Trans. Wirel. Commun.* **2020**, *19*, 6844–6857.
9. Gussen, C.M.G.; Diniz, P.S.R.; Campos, M.L.R.; Martins, W.A.; Costa, F.M.; Gois, J.N. A survey of underwater wireless communication technologies. *J. Commun. Inf. Syst.* **2016**, *31*(1).
10. Wang, H.; Sun, Z.; Guo, H.; Wang, P.; Akyildiz, I.F. Designing acoustic reconfigurable intelligent surface for underwater communications. *IEEE Trans. Wirel. Commun.* **2023**, *22*, 8934–8948.
11. Theocharidis, T.; Kavallieratou, E. Underwater communication technologies: A review. *Telecommun. Syst.* **2025**, *88*, 54. DOI: 10.1007/s11235-025-01279-x
12. Leccese, F.; Spagnolo, G.S. State-of-the-art and perspectives of underwater optical wireless communications. *Acta IMECO* **2021**, *10*(4), 25–35.
13. Gkoura, L.K.; Roumelas, G.D.; Nistazakis, H.E.; Sandalidis, H.G.; Vavoulas, A.; Tsigopoulos, A.D.; Tombras, G.S. Underwater Optical Wireless Communication Systems: A Concise Review. In *Turbulence Modelling Approaches*; Volkov, K., Ed.; IntechOpen: London, UK, 2017.
14. Cai, R.; **Zhang**, M.; Dai, D.; Shi, Y.; Gao, S. Analysis of the underwater wireless optical communication channel based on a comprehensive multiparameter model. *Appl. Sci.* **2021**, *11*(13), 6051.
15. NOAA Ocean Explorer Deep-light diagram. Available online: https://deepoceaneducation.org/wp-content/uploads/2021/10/diagram3_600.jpg
16. Tian, R.; Wang, T.; Shen, X.; Zhu, R.; Jiang, L.; Lu, Y.; Lu, H.; Song, Y.; Zhang, P. 108 m underwater wireless optical communication using a 490 nm blue VECSEL and an AOM. *Sensors* **2024**, *24*, 2609. DOI: 10.3390/s24082609
17. Zhang, M.; Zhou, H. Real-time underwater wireless optical communication system based on LEDs and estimation of maximum communication distance. *Sensors* **2023**, *23*(17), 7649.
18. Li, J.; et al. Single-photon detection for MIMO underwater wireless optical communication. *Opt. Express* **2021**, *29*(16), 25922–25937.
19. Ch, X.; Shen, Y.; Guo, H.; Oubei, H.M.; Ng, T.K.; Liu, G.; Park, K.H.; Ho, K.T.; Alouini, M.S.; Ooi, B.S. 20-meter underwater wireless optical communication link with 1.5 Gbps data rate. *Opt. Express* **2016**, *24*, 25502–25509.
20. Wang, J.; Lu, C.; Li, S.; Xu, Z. 100 m/500 Mbps underwater optical wireless communication using an NRZ-OOK modulated 520 nm laser diode. *Opt. Express* **2019**, *27*, 12171–12181.
21. Florida State University. Photomultiplier tube image. Available online: https://micro.magnet.fsu.edu/primer/digitalimaging/concepts/images/photomultiplier.jpg. (accessed on 20.05.2026)
22. Hamamatsu. Photomultiplier Tube; Available online: https://www.hamamatsu.com.cn/content/dam/hamamatsu-photonics/sites/documents/99_SALES_LIBRARY/etd/PMT_handbook_v4E.pdf. (accessed on 20.05.2026)
23. McIntyre, R.J. Multiplication noise in uniform avalanche diodes. *IEEE Trans. Electron Devices* **1966**, *ED-13*(1), 164–168.
24. Lehmann, A. Status and perspectives of vacuum-based photon detectors. *Nucl. Instrum. Methods Phys. Res. A* **2023**, *1056*, 168568.
25. Itzler, M.A.; et al. Single photon avalanche diodes (SPADs) for 1.5 μm photon counting applications. *J. Mod. Opt.* **2007**, *54*(2–3), 283–304.
26. Liu, Z.; An, N.; Han, X.; Nuñez, N.E.; Jin, L.; Liu, C. Progress in Avalanche Photodiodes for Laser Ranging. *Sensors* **2025**, 25, 2802. https://doi.org/10.3390/s25092802.
27. Windischhofer, P.; Riegler, W. Passive quenching, signal shapes, and space charge effects in SPADs and SiPMs. *Nucl. Instrum. Methods Phys. Res. A* **2023**, *1045*, 167627.

 doi:10.20944/preprints202606.0076.v1

28. Stipčević, M.; Christensen, B.G.; Kwiat, P.G.; Gauthier, D.J. Advanced active quenching circuit for ultra-fast quantum cryptography. *Opt. Express* **2017**, *25*(18), 21861.
29. Cox, W.C., Jr. *A 1 Mbps Underwater Communication System Using a 405 nm Laser Diode and Photomultiplier Tube*; Master's Thesis, North Carolina State University, 2008.
30. Hamza, T.; Khalighi, M.-A.; Bourennane, S.; Leon, P.; Opderbecke, J. On the suitability of employing silicon photomultipliers for underwater wireless optical communication links. In *Proceedings of CSNDSP 2016*; Prague, Czech Republic, 2016; pp. 1–5.
31. Fei, C.; Wang, Y.; Du, J.; Chen, R.; Lv, N.; Zhang, G.; Tian, J.; Hong, X.; He, S. 100-m/3-Gbps underwater wireless optical transmission using a wideband photomultiplier tube (PMT). *Opt. Express* **2022**, *30*(2), 2326–2337.
32. Rogalski, A.; Bielecki, Z.; Mikołajczyk, J. Detection of optical radiation. In *Handbook of Optoelectronics*; Taylor & Francis Group: Boca Raton, FL, USA, 2015.
33. Liu, W.; Zhang, L.; Huang, N.; Xu, Z. Wide dynamic range signal detection for underwater optical wireless communication using a PMT detector. *Opt. Express* **2023**, *31*(15), 25267–25279.
34. Ge, W.; Song, G.; Qin, S.; Zhang, Y.; Du, Z.; Xu, J. Weak signal detection based on pulse-width counting method for underwater wireless optical communication with an analog-mode PMT detector. *Opt. Express* **2024**, *32*(13), 23404–23415.
35. Han, X.; Li, P.; Li, G.; Chang, C.; Jia, S.; Xie, Z.; Liao, P.; Nie, W.; Xie, X. Demonstration of 12.5 Mslot/s 32-PPM underwater wireless optical communication system with 0.34 photons/bit receiver sensitivity. *Photonics* **2023**, *10*, 451.
36. Li, J.; Ye, D.; Fu, K.; Wang, L.; Piao, J.; Wang, Y. Photon-counting schemes for MIMO underwater wireless optical communication with arrayed PMTs. *Appl. Opt.* **2022**, *61*(2), 403–413.
37. Rogalski, A.; Bielecki, Z. *Detection of Optical Signals*; CRC Press: Boca Raton, FL, USA, 2022.
38. Wang, J.; et al. Underwater wireless optical communication system using a 16-QAM modulated 450-nm laser diode based on an FPGA. *Appl. Opt.* **2019**, *58*(16), 4553–4559.
39. Li, J.; et al. Large-coverage underwater visible light communication system based on blue LED employing equal-gain combining with integrated PIN array reception. *Appl. Opt.* **2019**, *58*, 383–388.
40. Wang, F.; et al. High-speed underwater visible light communication system based on LED employing maximum-ratio combination with multi-PIN reception. *Opt. Commun.* **2018**, *425*, 106–112.
41. Fei, C.; et al. 16.6 Gbps data rate for underwater wireless optical transmission with single laser diode achieved with discrete multi-tone and post-nonlinear equalization. *Opt. Express* **2018**, *26*, 34060–34069.
42. Liu, X.; Yi, S.; Zhou, X.; Fang, Z.; Qiu, Z.-J.; Hu, L.; Cong, C.; Zheng, L.; Liu, R.; Tian, P. 34.5 m underwater optical wireless communication with 2.70 Gbps data rate based on a green laser diode with NRZ-OOK modulation. *Opt. Express* **2017**, *25*(22), 27937–27947.
43. Lyu, W.; Zhao, M.; Chen, X.; Yang, X.; Qiu, Y.; Tong, Z.; Xu, J. Experimental demonstration of an underwater wireless optical communication employing spread-spectrum technology. *Opt. Express* **2020**, *28*(7), 10027–10038.
44. Lyu, W.; Li, X.; Zhang, Y.; Guan, X.; Zhang, Z.; Xu, J. Experimental demonstration of underwater wireless optical OFDM communication system with a single SPAD receiver. *Opt. Commun.* **2022**, *508*
45. Wang, J.; Yang, X.; Lv, W.; Yu, C.; Wu, J.; Zhao, M.; Qu, F.; Xu, Z.; Han, J.; Xu, J. Underwater wireless optical communication based on multi-pixel photon counter and OFDM modulation. *Opt. Commun.* **2019**, *451*, 181–185.
46. Sabbagh, A.G. Long-range underwater optical wireless communication systems in turbulent conditions. *Opt. Express* **2023**, *31*, 21311–21329.
47. Yan, Q.; Li, Z.; Hong, Z.; Zhan, T.; Wang, Y. Photon-counting underwater wireless optical communication by recovering clock and data from discrete single-photon pulses. *IEEE Photon. J.* **2019**, *11*(5), 7905815.
48. Yang, H.; Yan, Q.; Wang, M.; Wang, Y.; Li, P.; Wang, W. Synchronous clock recovery of photon-counting underwater optical wireless communication based on deep learning. *Photonics* **2022**, *9*, 884.
49. Shen, J.; Wang, J.; Yu, C.; Chen, X.; Wu, J.; Zhao, M.; Qu, F.; Xu, Z.; Han, J.; Xu, J. Single LED-based 46-m underwater wireless optical communication enabled by a multi-pixel photon counter with digital output. *Opt. Commun.* **2019**, *438*, 78–82.

 doi:10.20944/preprints202606.0076.v1

50. Zhao, M.; Li, X.; Chen, X.; Tong, Z.; Lyu, W.; Zhang, Z.; Xu, J. Long-reach underwater wireless optical communication with relaxed link alignment enabled by optical combination and arrayed sensitive receivers. *Opt. Express* **2020**, *28*(23), 34450–34460.
51. Wang, H.; Wang, L.; Wu, X.; Peng, H.; Liao, W.; Cai, C.; Song, G.; Du, Z.; Zhang, Z.; Fei, L.; Xu, J. A real-time MPPC-based duplex UWOC system. *J. Lightwave Technol.* **2025**, *43*(18), 8737–8746.
52. Shen, J.; Wang, J.; Chen, X.; Zhang, C.; Kong, M.; Tong, Z.; Xu, J. Towards power-efficient long-reach underwater wireless optical communication using a multi-pixel photon counter. *Opt. Express* **2018**, *26*(18), 23565–23571.
53. Chen, X.; Yang, X.; Tong, Z.; Dai, Y.; Li, X.; Zhao, M.; Zhang, Z.; Zhao, J.; Xu, J. 150 m/500 Mbps underwater wireless optical communication enabled by sensitive detection and receiver-side partial-response shaping with TCM. *J. Lightwave Technol.* **2021**, *39*(14), 4614–4621.
54. Dai, Y.; Chen, X.; Yang, X.; Tong, Z.; Du, Z.; Lyu, W.; Zhang, C.; Zhang, H.; Zou, H.; Cheng, Y.; Ma, D.; Zhao, J.; Zhang, Z.; Xu, J. 200-m/500-Mbps underwater wireless optical communication system utilizing a sparse nonlinear equalizer with variable-step-size GOMP. *Opt. Express* **2021**, *29*(20), 32228–32243.
55. Chi, N.; Zhao, Y.; Shi, M.; Zou, P.; Lu, X. Gaussian-kernel-aided deep neural network equalizer utilized in underwater PAM8 visible light communication system. *Opt. Express* **2018**, *26*(20), 26700–26712.
56. Zhao, Y.; Zou, P.; Chi, N. 3.2 Gbps underwater visible light communication system utilizing dual-branch multi-layer perceptron-based post-equalizer. *Opt. Commun.* **2020**, *460*, 125197.
57. Li, C.-Y.; Lu, H.-H.; Tsai, W.-S.; Lu, Y.-F. A 5 m/25 Gbps underwater wireless optical communication system. *IEEE Photon. J.* **2018**.
58. Fei, C.; Hong, X.; Zhang, G.; et al. Improving the performance of long-reach UWOC with multiband DFT-spread DMT. *IEEE Photon. Technol. Lett.* **2019**, *31*(16), 1315–1318.
59. Yang, Y.; Fan, L.; He, F.; Song, Y.; Duan, Z.; Zhu, Y.; Li, B. Long-distance underwater optical wireless communication with PPLN wavelength conversion. In *Proc. SPIE 11717*, 117172J (2020).
60. Dong, X.; Zhang, K.; Sun, C.; Zhang, J.; Zhang, A.; Wang, L. Towards 250-m gigabits-per-second underwater wireless optical communication using a low-complexity ANN equalizer. *Opt. Express* **2025**, *33*, 2321–2337.
61. Zhang, H.; Liu, X.; Dong, J.; Yu, H.; Zhou, C.; Zhang, B.; Xu, Y.; Jie, W. Centimeter-sized inorganic lead halide perovskite $CsPbBr_3$ crystals grown by an improved solution method. *Cryst. Growth Des.* **2017**, *17*, 6426–6431.
62. He, L.; Li, M.; Chen, Q.; Sun, R.; Wang, F.; Wang, X.; Wu, H.; Wei, W.; Qin, T.; Shen, L. Self-powered and low-noise perovskite photodetector enabled by a novel dopant-free hole-transport material with bottom passivation for underwater blue light communications. *ACS Appl. Mater. Interfaces* **2022**, *14*, 46809–46818.
63. Zhou, X.; Luo, L.; Huang, Y.; Wei, S.; Zou, J.; He, A.; Huang, B.; Li, X.; Zhao, J.; Shen, K.; et al. Macroscopic and microscopic defect management in blue/green photodetectors for underwater wireless optical communication. *J. Mater. Chem. C* **2022**, *10*, 5970–5980.
64. Yu, D.; Cao, F.; Gu, Y.; Han, Z.; Liu, J.; Huang, B.; Xu, X.; Zeng, H. Broadband and sensitive two-dimensional halide perovskite photodetector for full-spectrum underwater optical communication. *Nano Res.* **2020**, *14*, 1210–1217.
65. Wei, J.; Deng, Y.; Fei, J.; Yang, T.; Chen, P.; Zhu, L.; Huang, Z. Solution-processed $CsPbBr_3$ perovskite photodetectors for cost-efficient underwater wireless optical communication system. *Micromachines* **2024**, *15*, 1185.
66. Zhang, B.; Wang, J.; Liu, G.; et al. A strongly coupled Ru–CrOx cluster–cluster heterostructure for efficient alkaline hydrogen electrocatalysis. *Nat. Catal.* **2024**, *7*, 441–451.
67. Zhang, J.; Jiao, S.; Wang, D.; Gao, S.; Wang, J.; Zhao, L. Nano tree-like branched structure with α-Ga_2O_3 covered by γ-Al_2O_3 for highly efficient detection of solar-blind ultraviolet light using self-powered photoelectrochemical method. *Appl. Surf. Sci.* **2021**, *541*, 148380.
68. Dong, R.; Wang, H.; Zhang, J.; et al. Self-powered SiC-based photoelectrochemical ultraviolet photodetectors for robust underwater optical communication against full aquatic environments. *Adv. Sci.* **2026**, *13*, e13939.
69. Guo, Y.; et al. Current trend in optical Internet of Underwater Things. *IEEE Photon. J.* **2022**, *14*(5), 7350414.

 doi:10.20944/preprints202606.0076.v1

70. Zhang, H.; Dong, Y.; Hui, L. On capacity of downlink underwater wireless optical MIMO systems with random sea surface. *IEEE Commun. Lett.* **2015**, *19*(12), 2166–2169.
71. Hu, S.; Mi, L.; Zhou, T.; Chen, W. 35.88 attenuation lengths and 3.32 bits/photon underwater optical wireless communication based on photon-counting receiver with 256-PPM. *Opt. Express* **2018**, *26*(17), 21685–21699.
72. Khalighi, M.; Hamza, T.; Bourennane, S.; Léon, P.; Opderbecke, J. Underwater wireless optical communications using silicon photomultipliers. *IEEE Photon. J.* **2017**, *9*(4), 7905310.
73. Guo, Y. Compact scintillating-fiber/450-nm-laser transceiver for full-duplex underwater wireless optical communication system under turbulence. *Opt. Express* **2022**, *30*(1), 53–69.
74. Kang, C.H. Ultraviolet-to-blue color-converting scintillating-fibers photoreceiver for 375-nm laser-based underwater wireless optical communication. *Opt. Express* **2019**, *27*(21), 30450–30461.
75. Sait, M. Dual-wavelength luminescent fibers receiver for wide field-of-view, Gb/s underwater optical wireless communication. *Opt. Express* **2021**, *29*(23), 38014–38026.
76. Kong, M. Survey of energy-autonomous solar cell receivers for satellite–air–ground–ocean optical wireless communication. *Prog. Quantum Electron.* **2020**, *74*, 100300.
77. Kong, M. Underwater wireless optical communication using a lens-free solar panel receiver. *Opt. Commun.* **2018**, *426*, 94–98.
78. Trichili, A.; Issaid, C.B.; Ooi, B.S.; Alouini, M.-S. CNN-based structured light communication scheme for Internet of Underwater Things applications. *IEEE Internet Things J.* **2020**, *7*(10), 10038–10047.
79. Mangeret, R.; Farenc, J.; Ai, B.; Destruel, P.; Puretolas, D.; Casanovas, J. Optical detection of partial discharges using fluorescent fiber. *IEEE Trans. Electr. Insul.* **1991**, *26*(4), 783–789.
80. Farenc, J.; Mangeret, R.; Boulanger, A.; Destruel, P.; Lescure, M. A fluorescent plastic optical fiber sensor for detection of corona discharges in high-voltage electrical equipment. *Rev. Sci. Instrum.* **1994**, *65*(1), 155–160.
81. Peyronel, T.; Quirk, K.J.; Wang, S.C.; Tiecke, T.G. Luminescent detector for free-space optical communication. *Optica* **2016**, *3*(7), 787.
82. Kang, C.H.; et al. High-speed colour-converting photodetector with all-inorganic $CsPbBr_3$ perovskite nanocrystals for ultraviolet light communication. *Light Sci. Appl.* **2019**, *8*, 94.
83. Min, J.-W.; et al. Unleashing the potential of MBE-grown AlGaN-based ultraviolet nanowire devices. *J. Nanophoton.* **2018**, *12*(4), 043511.
84. Sang, L.; Liao, M.; Sumiya, M. A comprehensive review of semiconductor ultraviolet photodetectors: From thin films to one-dimensional nanostructures. *Sensors* **2013**, *13*(8), 10482–10518.
85. Chen, H.; Liu, K.; Hu, L.; Al-Ghamdi, A.A.; Fang, X. New-concept ultraviolet photodetectors. *Mater. Today* **2015**, *18*(9), 493–502.
86. Kim, S.-M.; Won, J.-S.; Nahm, S.-H. Simultaneous reception of solar power and visible light communication using a solar cell. *Opt. Eng.* **2014**, *53*(4), 046103.
87. Wang, Z.; Tsonev, D.; Videv, S.; Haas, H. Towards self-powered solar panel receiver for optical wireless communication. In *Proc. IEEE ICC*; 2014; pp. 3348–3353.
88. Shin, W.-H.; Yang, S.-H.; Kwon, D.-H.; Han, S.-K. Self-reverse-biased solar panel optical receiver for simultaneous visible light communication and energy harvesting. *Opt. Express* **2016**, *24*(22), A1300.
89. Kim, S.-M.; Won, J.-S. Simultaneous reception of visible light communication and optical energy using a solar cell receiver. In *Proc. ICTC*; 2013; pp. 896–897.
90. Zhang, S.; et al. Organic solar cells as high-speed data detectors for visible light communication. *Optica* **2015**, *2*(7), 607–610.
91. Fakidis, J.; Videv, S.; Helmers, H.; Haas, H. 0.5-Gb/s OFDM-based laser data and power transfer using a GaAs photovoltaic cell. *IEEE Photon. Technol. Lett.* **2018**, *30*(9), 841–844.
92. Kong, M.; Lin, J.; Kang, C.H.; et al. Toward self-powered and reliable visible light communication using amorphous silicon thin-film solar cells. *Opt. Express* **2019**, *27*, 34542–34551.
93. Sonardyne Ltd. Underwater communication systems. Available online: https://www.sonardyne.com/offer/communications (accessed on 20.05.2026).

 doi:10.20944/preprints202606.0076.v1

94. Lumasys. Underwater optical communication products. Available online: https://lumasys.com (accessed on 20.05.2026).
95. Hydromea SA. LUMA underwater optical communication. Available online: https://www.hydromea.com/luma-underwater-communication (accessed on 20.05.2026).